Full Paper

Propellants, Explosives, Pyrotechnics

DOI: 10.1002/prep.201800014

# High Catalytic Activity of Nitrogen-Doped Graphene on the Thermal Decomposition of CL-20

Ting Zhang,[a] Yu Guo,[a] Jiachen Li,[a] Yulei Guan,[a] Zhaoqi Guo,[a] and Haixia Ma*[a]

**Abstract:** Graphene based materials with excellent physical properties have attracted much attention in the field of energetic materials. Notably, heteroatom doping could modify the property of graphene. Herein, nitrogen-doped graphene (NGO) with a tunable hierarchical morphology and high surface areas was prepared by a hydrothermal method. NGO composites with 2,4,6,8,10,12-hexanitro-2,4,6,8,10,12-hexaazaisowurtzitane (CL-20) were obtained by recrystallization in ethyl acetate. Subsequently, the catalytic activities of NGO and undoped reduced graphene oxide (rGO) on the thermal decomposition of CL-20 were investigated using differential scanning calorimetry (DSC). The decomposition temperature, self-accelerating decomposition temperature, and thermal ignition temperature of CL-20 all decrease under the influence of NGO. This is attributed to change in charge distribution of carbon atoms influenced by nitrogen dopants and more active sites induced on graphene surface. As a result, NGO exhibits enhanced catalytic effect on the thermal decomposition of CL-20.

**Keywords:** Nitrogen doped graphene · Thermal decomposition · CL-20 · Catalytic activity

## 1 Introduction

High energy density, insensitivity, short ignition delay time and fast reaction rate are the decisive factors for evaluating the performance of propellants [1–2]. So far, many researchers have been working on improving techniques to enhance the combustion performance so as to meet the military and civilian needs. As we know, the thermal decomposition properties could directly influence the combustion characteristics of propellants. According to research reports, it is an effective and simple tool to regulate the thermal decomposition characteristics of propellant using combustion catalyst. Therefore, the development of new and highly efficient combustion catalysts has attracted wide attentions in recent years.

Carbon is one of the important additives since explosives were invented. It was found that the addition of carbon-based materials, such as: carbon black, fullerene and carbon nanotube, et al, could help to reduce electrostatic hazards, impact and friction sensitivity, or further regulate the combustion and detonation performance [3–9]. Among the various carbon materials, graphene draws great interest from people due to its excellent physical characteristics applied in various fields since it was first reported [9–12]. Graphene oxide (GO), a derivative of graphene, has large amount of oxygen containing functional groups on the carbon framework, endowing it strong hydrophilicity and surface activity. Moreover, GO can bring great changes on the thermal decomposition of 2,4,6,8,10,12-hexanitro-2,4,6,8,10,12-hexaazaisowurtzitane (CL-20 or HNIW), cyclotetramethylenete-tranitramine (HMX) or ammonium perchlorate (AP) comparing with pure energetic components [9,13–14]. In comparison with GO, rGO has few oxygen-containing groups, however, its conductive property is better than GO. Yu et al. studied a novel CL-20-based explosive formula with the decoration of rGO and obtained a lower sensitive energetic material [15]. Other than intrinsic properties of graphene, heteroatoms doping is an effective way to manipulate the properties for further expanding its application [16]. Zhang et al. had successfully prepared a nitrated GO by nitro substitution reaction and studied its thermal behavior on the decomposition of AP. The decomposition temperature of AP decreased by 106 °C and the heat release increased from 875 J/g to 3236 J/g [14]. Heteroatoms doping could affect the charge distribution and increase surface defects of GO, which result in an enhanced chemical reactive activity in the catalytic reaction [17]. It has been reported that NGO shows an exceptional behavior than undoped graphene in supercapacitors and photocatalytic activities and so on [18–19]. In view of the outstanding performance of NGO, it is interesting to study the catalytic pyrolysis effect on energetic materials.

CL-20 is a high energy density compound and has excellent detonation performance. Usually, CL-20 is used with other additives for enhancing its combustion property in the practical application [20–22]. Carbon materials play an important role in the combustion of propellant. On the one hand, carbon materials can be used to load metal and metal

[a] *T. Zhang, Y. Guo, J. Li, Y. Guan, Z. Guo, H. Ma*
*School of Chemical Engineering*
*Northwest University*
*Xi'an, 710069, P. R. China*
**e-mail: mahx@nwu.edu.cn*

  

oxides; on the other hand, it can promote the sufficient reaction of $NO_2$ released by the pyrolyzation of oxidant [23]. Combining the prominent effect of carbon material and the increased active region of NGO, it is worth to study the catalytic activity of NGO on the thermal decomposition of CL-20.

In this work, urea was used as nitrogen source for hydrothermal synthesis of NGO. And then, NGO/CL-20 composite was obtained by recrystallization process. Thermogravimetry-differential thermogravimetry (TG-DTG) and differential scanning calorimetry (DSC) techniques were used to investigate the thermal decomposition performance of NGO/CL-20. Furthermore, we also compared the different effect of rGO with NGO on the thermal decomposition of CL-20 for the first time.

## 2 Experimental Section

### 2.1 Reagents and Materials

Caution! CL-20 and the corresponding composites are explosive hazardous materials. The wearing of safety glasses and face shields is strongly recommended when handling these materials with large amount. The use of metal spatulas is strictly forbidden. Fire and static electricity discharge should be avoided. TG-DTG and DSC analyses should use no more than 2 mg sample to avoid instrument damage. Graphite was purchased from Shanghai Huayi Group Huayuan Chemical Co., Ltd. CL-20 was provided by Xi'an Modern Chemistry Research Institute.

### 2.2 Preparation of GO, rGO and NGO

According to the literature, GO was prepared by improved hummer's method [24]. The synthesis of NGO follows the procedure of reference [25]. Briefly, 40 mg GO was dispersed into 30 ml distilled water to form a homogeneous suspension, and then mixed with 12 g urea. After ultrasonic dispersion for 30 min, the solution was hydrothermally treated in a 40 ml Teflon-lined stainless autoclave at 180 °C for 12 h. The products were washed with distilled water and freeze-dried at −50 °C for 12 h. rGO was obtained following the same method without urea.

### 2.3 Preparation of NGO/CL-20 and rGO/CL-20

10 mg NGO was dispersed in ethyl acetate by ultrasonic method, then mixed with 40 mg CL-20. The mixture was stirred slowly for 10 min and then stored statically. The NGO/CL-20 composites could be obtained by slow evaporation of ethyl acetate at room temperature. For comparison, the preparation of rGO/CL-20 and graphite/CL-20 composites followed the same procedure.

### 2.4 Characterization

The phase identification was carried out using a Japan D/max-3C automatic X-ray diffraction apparatus with Cu Kα irradiation. Scanning electron microscopy (Zeiss SIGMA) and transmission electron microscope were used to detect the microstructure and morphology. Raman spectra were investigated on a Raman spectrometer (Renishaw Co., UK) within the range of 100–4000 $cm^{-1}$. The chemical compositions of samples were demonstrated by X-ray photoelectron spectroscopy ((K-alpha, Thermo Fisher). The thermal behaviors of the samples were tested using DSC (Q2000, TA) and simultaneous DSC-TGA (SDT, Q600, TA).

## 3 Results and Discussion

### 3.1 XRD and Raman Analysis

Figure 1 shows the XRD patterns of GO, rGO and NGO. A strong peak located at $2\theta = 11.7^\circ$ corresponds to the characteristic peak of GO [25]. In the XRD curves of NGO and rGO, the characteristic peak of GO disappears and a new peak located at $2\theta = 25^\circ$ can be observed clearly. These results indicated that the oxygen-containing functional groups were removed during the hydrothermal procedure [26].

Raman analysis, an effective method for structural analysis of materials, was used to distinguish the ordered and disordered carbon structures of graphene materials in present work. In Figure 1 (b), three characteristic curves represent three types of graphene materials, respectively. The D band and G band are two major feature bands of graphene materials. However, the flake graphite has a major peak in 1584.5 $cm^{-1}$, which indicates it has a complete lattice structure. When flake graphite is oxidized and stripped, a new characteristic peak (D band) appears at ~1350 $cm^{-1}$ [15]. Some carbon atoms in graphene skeleton convert into $sp^3$ hybridization from $sp^2$ hybridization. Compared with GO, the intensity ratio of D band and G band ($I_D/I_G$) increases apparently on NGO and rGO. This means the decrease of or-

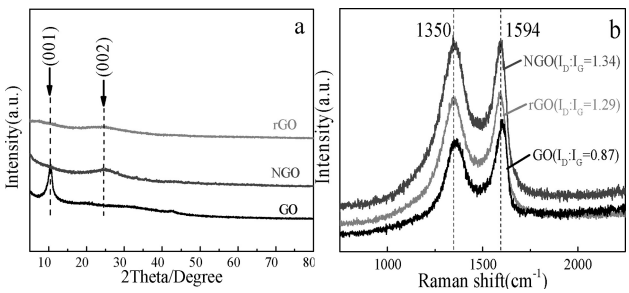


**Figure 1.** XRD spectra (a) and Raman spectra (b) of GO, rGO and NGO.

  

dered structure and the increase of defects under the hydrothermal process.

### 3.2 Structure and Composition

The structures of GO, rGO and NGO were characterized by the SEM and TEM (Figure 2). The SEM and TEM images of GO are shown in Figure 2a and d. The typical crimped structure can be observed, which may originate from the defects created in the oxidation process. Figure 2(b) explicitly shows the multilayer structure of rGO, which could be verified by TEM image (Figure 2(e)). In Figure 2(c), the rich porous structure of NGO may originate from the release of $NH_3$ gas from the decomposition of urea. TEM image (Figure 2(f)) reveals that NGO consists of few layers of graphene sheets.

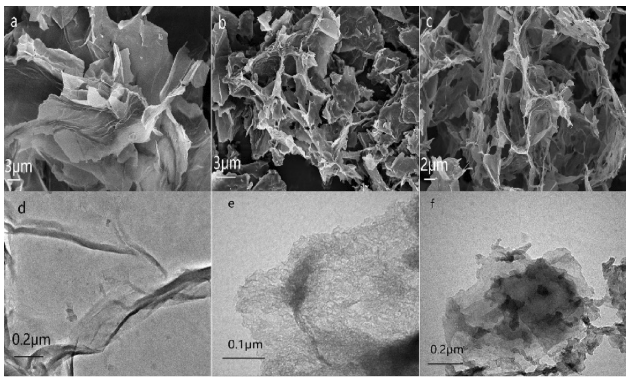


**Figure 2.** SEM and TEM micrographs of GO (a, d), rGO (b, e) and NGO (c, f).

XPS could accurately investigate the valence state and chemical structure of elements. It could be used to verify whether nitrogen atoms were introduced or not. As shown in Figure 3(a), the C 1s peak of the rGO exhibits one main peak (C–C) located at 284.6 eV and three small peaks, including the C–O bond at 285.3 eV, C=O bond at 286.4 eV and O–C=O bond at 288.8 eV [27]. Figure 3(b) shows the C 1s of NGO. The peak located at 286.4 eV for C=O increases after nitrogen doping, which ascribes to the overlap of the peaks of C=O with C–N. Compared with the C 1s of GO in Figure 3(c), all the peak intensity of functional groups of NGO or rGO obviously decreases after the hydrothermal reduction. Figure 3(d) shows the N 1s high-resolution XPS spectrum of NGO. According to the XPS investigation, the content of N element is about wt 3.29 %. The nitrogen peak could be fitted into three different peaks at 398.9 eV (pyridinic N), 400.1 eV (pyrrolic N), and 401.5 eV (graphitic N), respectively, which further indicates that the nitrogen atoms of urea are successfully introduced into the graphene skeleton via the hydrothermal reaction [28].

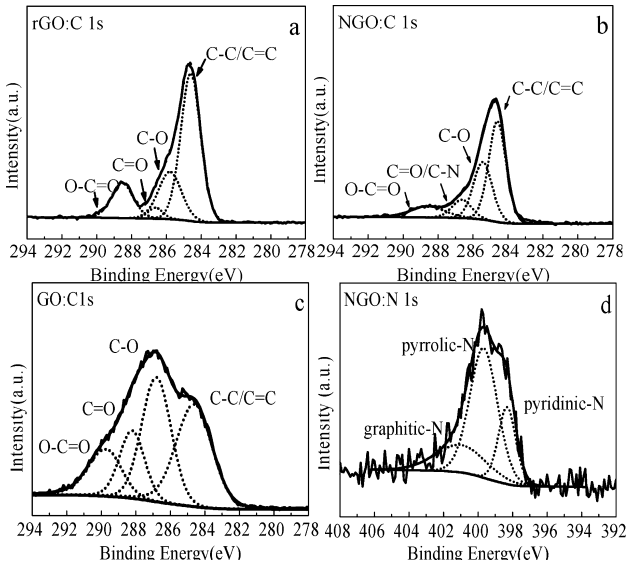


**Figure 3.** High-Resolution XPS spectra of samples: C1s of rGO (a); C1s of NGO (b); C1s of GO (c) and N1s of NGO (d).

### 3.3 Catalytic Performance

DSC is an effective method to study the thermal behavior of energetic materials. Basing on the decomposition peak temperature ($T_p$) of the mixed components, we can estimate the catalytic effect of different additives on the thermal decomposition of CL-20 from the temperature difference.

Figure 4 (a) is the XRD spectra of pure CL-20 and NGO/CL-20 composite, which all exactly match with the standard card (JCPD#50-2045). There is no impurity peak in the diagram, indicating that the recrystallization process does not change the crystal structure of CL-20. As shown in Figure 4(b), it can be seen that the NGO/CL-20 composite has a strong exothermic peak at 245.63 °C, and the composite of graphite/CL-20 has an exothermic peak temperature at 247.67 °C at the heating rate of 10 °C/min, which are lower than the pure CL-20. However, the pure NGO has no exothermic peak. As shown in Figure 5, the DSC curves of CL-20, rGO/CL-20 and NGO/CL-20 all show one strong exother-

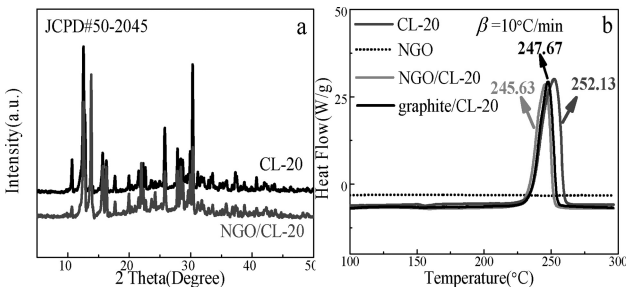


**Figure 4.** The XRD spectra of pure CL-20 and NGO/CL-20 (a); DSC curves of CL-20, NGO and NGO/CL-20 (b).

  

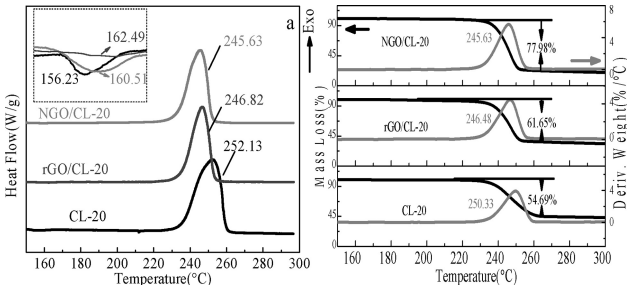


**Figure 5.** DSC (a) and TG-DTG (b) curves of three samples at a heat rate of 10 °C/min.

mic peak, which corresponds to the abrupt mass loss stage shown in their respective TG-DTG curves (Figure 5(b)). The variation trend of peak temperatures in DTG curves is consistent with their DSC curves. In Figure 5(a), the DSC curve of CL-20 shows one tiny endothermic peak at 156.23 °C owing to the conversion of ε to ϒ phase (inserted graph) and one strong exothermic decomposition process with a peak temperature of 252.13 °C. Other two decomposition peak temperatures of NGO/CL-20 and rGO/CL-20 are 245.63 and 246.82 °C, respectively. Notably, the crystalline transformation process of both NGO/CL-20 and rGO/CL-20 can be observed. Compared with pure CL-20, both NGO and rGO have a certain extent of catalytic effects on accelerating the thermal decomposition of CL-20. Nevertheless, NGO exhibits a better catalytic effect than rGO, with the reducing of the exothermic decomposition peak temperature by 6.5 °C.

The apparent activation energy ($E_a$) of the exothermic decomposition reaction is a vital parameter for evaluating the catalytic effect of a catalyst. The DSC curves at four different heating rates of 5.0, 7.5, 10, and 12.5 °C/min were obtained [29–30]. We calculated the activation energies of NGO/CL-20 corresponding to different reactive degree ($\alpha$) by Ozawa method and the curves of $E$-$\alpha$ are shown in Figure 6. Moreover, an integral iso-conversional non-linear (NL-INT) method was used to ensure the accuracy of the values of $E$ [30]. The equations involved in the above calculations are as follow:

$$\text{Kissinger equation}: \quad \frac{\mathrm{d}\ln\frac{\beta}{T_p^2}}{\mathrm{d}\frac{1}{T_p}} = -\frac{E}{R}$$

$$\text{Ozawa equation}: \quad \lg\beta + \frac{0.4576E}{RT} = C$$

$$\text{NL}-\text{INT equation}: \Omega_{1l} = \min\left|\sum_{i=1}^{n}\sum_{j\neq i}^{n}\frac{\beta_j \cdot I(E_\alpha, T_{\alpha,i})}{\beta_i \cdot I(E_\alpha, T_{\alpha,j})} - n(n-1)\right|$$

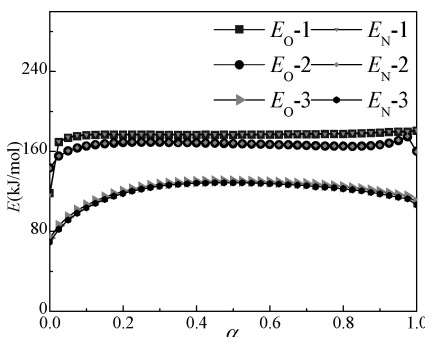


**Figure 6.** $E$-$\alpha$ curves of three different samples ($E_O$ and $E_N$ are obtained by Ozawa method and integral iso-conversional non-linear (NL-INT) method, respectively. 1,2 and 3 represents CL-20, rGO/CL-20 and NGO/CL-20, respectively.)

As shown in Figure 6, the values of $E$ of NGO/CL-20 are relatively uniform over the range of $\alpha$ from 0.275 to 0.825, which could be used to calculate the relative kinetic parameters and study the most probable kinetic model function ($f(\alpha)$) of the intense exothermal reaction.

The corresponding experimental data from DSC curves and forty-one types of kinetic model functions were put into five integral equations (General, Universal, MacCallum-Tanner, Šatava-Šesták and Agrawal) for further mathematical calculation, respectively [31]. The detailed results are shown in Table 1. The mean values of kinetic parameters obtained by logical choice method are close to that obtained by Kissinger method and Ozawa method, which further demonstrates that the values of $E_a$ are reliable. Besides, the most probable kinetic model function of the exothermic decomposition reaction of NGO/CL-20 is classified as the Avrami-Erofeev equation: $f(\alpha)=3(1-\alpha)[-\ln(1-\alpha)]^{2/3}$. Substituting $f(\alpha)$, $E_a$ with 154.57 kJ mol$^{-1}$ and $A$ with $10^{13.40}$ s$^{-1}$ into equation 1.

$$\frac{d\alpha}{dT} = \frac{A}{\beta} f(\alpha)e^{-E/RT} \tag{1}$$

Herein, the kinetic equation of the exothermic decomposition reaction of NGO/CL-20 can be described as follows:

$$\frac{\mathrm{d}\alpha}{\mathrm{d}T} = \frac{10^{13.40}}{\beta}3(1-\alpha)[-\ln(1-\alpha)]^{2/3}\exp(-154570/RT)$$

For comparison, the exothermic reaction mechanisms of rGO/CL-20 and CL-20 were analyzed and the results indicating that they follow the same mechanism function model.

Both apparent activation energy and thermal decomposition temperature of NGO/CL-20 are lower than those of rGO/CL-20 and CL-20. A probable mechanism is the charge distribution of carbon atoms in NGO can be influenced by their neighboring nitrogen, which could induce more active regions and further enhance its chemical reactive activity [32]. Meanwhile, the porous structure of NGO supplies abundant active surfaces to accommodate energetic components. Thus, NGO, as a new carbon material, acting as a catalyst in propellant, which can also reduce the sensitivity

  

**Table 1.** Thermal decomposition kinetic parameters of NGO/CL-20, rGO/CL-20 and CL-20.

| Samples | | NGO/CL-20 | | | rGO/CL-20 | | | CL-20 | | |
|---|---|---|---|---|---|---|---|---|---|---|
| Method | $\beta$ | $E_a$ | log$A$ | $r$ | $E_a$ | log$A$ | $r$ | $E_a$ | log$A$ | $r$ |
| General | 5 | 154.79 | 13.74 | 0.9977 | 166.92 | 14.87 | 0.9993 | 179.10 | 15.99 | 0.9901 |
| | 7.5 | 160.07 | 14.22 | 0.9990 | 176.58 | 15.87 | 0.9992 | 182.43 | 16.36 | 0.9934 |
| | 10 | 157.42 | 13.95 | 0.9999 | 182.27 | 16.46 | 0.9995 | 163.62 | 14.40 | 0.9918 |
| | 12.5 | 145.15 | 12.66 | 0.9996 | 159.38 | 14.09 | 0.9997 | 184.18 | 16.51 | 0.9929 |
| Universal | 5 | 154.06 | 12.41 | 0.9976 | 166.26 | 13.51 | 0.9993 | 178.45 | 14.61 | 0.9901 |
| | 7.5 | 159.49 | 12.90 | 0.9990 | 176.02 | 14.50 | 0.9992 | 181.85 | 14.98 | 0.9933 |
| | 10 | 156.90 | 12.64 | 0.9999 | 181.77 | 15.09 | 0.9995 | 163.11 | 13.07 | 0.9917 |
| | 12.5 | 144.71 | 11.39 | 0.9996 | 158.94 | 12.78 | 0.9997 | 183.73 | 15.14 | 0.9929 |
| MacCallum-Tanner | 5 | 155.71 | 13.79 | 0.9979 | 167.99 | 14.93 | 0.9994 | 180.26 | 16.07 | 0.9910 |
| | 7.5 | 161.16 | 14.29 | 0.9999 | 177.80 | 15.95 | 0.9993 | 183.68 | 16.45 | 0.9940 |
| | 10 | 158.54 | 14.02 | 0.9999 | 183.59 | 16.56 | 0.9995 | 164.80 | 14.48 | 0.9926 |
| | 12.5 | 146.25 | 12.72 | 0.9997 | 160.59 | 14.16 | 0.9999 | 185.56 | 16.62 | 0.9935 |
| Šatava-Šesták | 5 | 155.20 | 13.77 | 0.9979 | 166.79 | 14.84 | 0.9994 | 178.38 | 15.91 | 0.9910 |
| | 7.5 | 160.34 | 14.23 | 0.9999 | 176.05 | 15.80 | 0.9993 | 181.61 | 16.26 | 0.9940 |
| | 10 | 157.87 | 13.98 | 0.9999 | 181.52 | 16.37 | 0.9995 | 163.78 | 14.40 | 0.9926 |
| | 12.5 | 146.27 | 12.76 | 0.9996 | 159.80 | 14.11 | 0.9999 | 183.38 | 16.42 | 0.9935 |
| Agrawal | 5 | 154.79 | 13.74 | 0.9977 | 166.92 | 14.86 | 0.9993 | 179.10 | 15.99 | 0.9901 |
| | 7.5 | 160.07 | 14.22 | 0.9990 | 176.58 | 15.86 | 0.9992 | 182.43 | 16.36 | 0.9934 |
| | 10 | 157.42 | 13.95 | 0.9999 | 182.27 | 16.46 | 0.9995 | 163.62 | 14.40 | 0.9918 |
| | 12.5 | 145.15 | 12.66 | 0.9996 | 159.38 | 14.09 | 0.9997 | 184.18 | 16.51 | 0.9929 |
| Mean | | 154.57 | 13.40 | | 171.37 | 15.06 | | 177.36 | 15.55 | |
| Kissinger | | 160.79($E_K$) | 14.27 | 0.9977 | 171.73($E_K$) | 15.35 | 0.9937 | 183.38($E_K$) | 16.37 | 0.9951 |
| Ozawa | | 161.05($E_O$) | | 0.9980 | 171.48($E_O$) | | 0.9942 | 182.65($E_O$) | | 0.9955 |

Note: $\beta$ is the heating rate. $T_p$ is the exothermic peak temperature. $E_K$ and $E_O$ are obtained from the $T_p$ by Kissinger method and Ozawa method, respectively. $r$ is the linear correlation coefficient. $R$ is the ideal gas constant ($R=8.314$ J/mol·K). $A$ is the pre-exponential factor.

of energetic materials [23, 33], promotes the decomposition reaction of CL-20.

### 3.4 Thermal Safety

The self-accelerating decomposition temperature ($T_{SADT}$ or $T_{e0}$) thermal ignition temperature ($T_{be0}$ or $T_{TIT}$) and critical thermal explosion temperature ($T_b$) are important parameters for evaluating thermal safety of energetic materials. The $T_{be0}$ and $T_b$ of NGO/CL-20, rGO/CL-20 and CL-20 were calculated by Zhang-Hu-Xie-Li's equation [equation (2)] [34].

$$T_{be0(or\ bp0)} = \frac{E_O - \sqrt{E_O^2 - 4E_O R T_{e0(or\ p0)}}}{2R} \quad (2)$$

$$T_{ei(or\ pi)} = T_{eo(or\ po)} + a\beta_i + b\beta_i^2 \quad i = 1 \sim 4 \quad (3)$$

Where the $T_{e0}$ and $T_{p0}$ corresponding to $\beta \to 0$ were calculated from equation (3). $E_{eO}$ and $E_{pO}$ could be obtained by substituting onset temperature ($T_e$) and peak temperature ($T_p$) into Ozawa equation, respectively. $a$ and $b$ are coefficients.

Besides, the corresponding entropy of activation ($\Delta S^{\neq}$), enthalpy of activation ($\Delta H^{\neq}$), and free energy of activation ($\Delta G^{\neq}$) of the decomposition reaction were obtained by Equation 4 ~ 6.

$$A = \frac{k_B T}{h} e^{\Delta S^{\neq}/R} \quad (4)$$

$$\Delta H^{\neq} = E_a - RT \quad (5)$$

$$\Delta G^{\neq} = \Delta H^{\neq} - T\Delta S^{\neq} \quad (6)$$

Where $T=T_{p0}$, $E_a=E_K$ and $A=A_K$. $k_B$ is the Boltzmann constant ($1.381\times10^{-23}$ J K$^{-1}$) and $h$ is the Planck constant ($6.626\times10^{-34}$ J s) [29]. All the calculated thermal parameters are listed in Table 2.

**Table 2.** Calculated values of kinetic parameters of decomposition reaction for the samples.

| Samples | | CL-20 | rGO/CL-20 | NGO/CL-20 |
|---|---|---|---|---|
| $T_{e0}$ ($T_{SADT}$) | °C | 222.21 | 217.41 | 211.58 |
| $T_{be0}$ ($T_{TIT}$) | °C | 233.70 | 228.46 | 224.73 |
| $T_{p0}$ | °C | 234.25 | 222.82 | 220.90 |
| $T_{bp0}$ ($T_b$) | °C | 246.54 | 235.28 | 234.19 |
| $\Delta S^{\neq}$ | J/mol/K | 63.97 | 45.10 | 23.99 |
| $\Delta H^{\neq}$ | kJ/mol | 179.17 | 167.81 | 156.68 |
| $\Delta G^{\neq}$ | kJ/mol | 146.71 | 145.44 | 144.83 |

The $T_{TIT}$ and $T_b$ of CL-20, rGO/CL-20 and NGO/CL-20 decrease progressively. Figure 7 clearly shows the variation trend of thermal safety parameters of three samples. The $\Delta G^{\neq}$ of NGO/CL-20 decreases compared with that of CL-20,

  

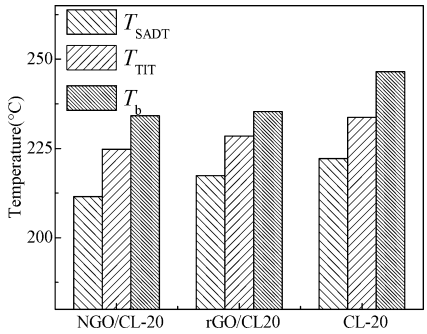


**Figure 7.** The kinetic parameters of NGO/CL-20, rGO/CL-20 and CL-20.

indicating that CL-20 is easier to decompose when CL-20 is incorporated into NGO. On the one hand, graphene has excellent thermal conductivity. On the other hand, the increased charge density and active regions by nitrogen doping could accelerate the break of nitro-group in the thermal decomposition reaction of CL-20 [35]. Comprehensively considering the decomposition peak temperature, the apparent activation energy, the self-accelerating decomposition temperature, thermal ignition temperature and critical thermal explosion temperature, NGO is a better combustion catalyst for the thermal decomposition of CL-20.

Notably, before the large-scale isothermal experiments in accordance with United Nations standards [36–37], small-scale trials of all prepared samples performed by non-isothermal DSC method in our experiment, have the advantage of fast selecting samples with better thermal decomposition performance. This could save the time, material resources and financial resources.

## 4 Conclusion

In summary, nitrogen-doped graphene was prepared by a hydrothermal method and its catalytic activity on thermal decomposition of CL-20 was investigated. Benefitting from the nitrogen atoms, more surface defects and active sites were created, which can enhance the thermal decomposition reaction of energetic materials. The apparent activation energy and thermal decomposition temperature of NGO/CL-20 decrease by 22.79 kJ/mol and 6.5 °C, respectively, which indicates that NGO promotes the self-accelerating decomposition reaction of CL-20. Besides, the thermal decomposition reaction mechanism of NGO/CL-20 was studied and can be classified with the Avrami-Erofeev equation (No.11): $f(\alpha)=3(1-\alpha)\ [-\ln(1-\alpha)]^{2/3}$. With the excellent catalytic performance of NGO, this work could stimulate further research in this area.

## *Acknowledgements*

This work is supported by the National Natural Science Foundation of China (Nos. 21373161, 21673179, 21504067), and Overseas Students Science and Technology Activities Project Merit Funding from Shaanxi, China.

## References

[1] F. Monteilrivera, L. Paquet, S. Deschamps, V. K. Balakrishnan, C. Beaulieu, J. Hawari, Physico-chemical measurements of CL-20 for environmental applications comparison with RDX and HMX, *J. Chromatogr. A* **2004**, *1025*, 125–132.

[2] D. C. Sorescu, B. M. Rice, D. L. Thompson, Theoretical studies of the hydrostatic compression of RDX, HMX, HNIW, and PETN crystals, *J. Phys. Chem. B* **1999**, *103*, 6783–6790.

[3] P. Wang, Effects of carbon black on burning properties of plateau double base propellant with low flame temperature, *J. Solid Rocket Techno.* **1996**, *19*, 38–42.

[4] F. Gao, S. F. LI, Approach to the catalytic mechanism of fullerene in propellants, *J. Energ. Mater.* **2003**, *21*, 33–41.

[5] X. Han, T. F. Wang, Z. K. Lin, D. L. Han, S. F. LI, RDX/AP-CMDB Propellants containing fullerenes and carbon black additives, *Def. Sci. J.* **2009**, *59*, 284–293.

[6] J. E. Um, T. Yeo, W. Choi, J. S. Chae, H. S. Kim, W. J. Kim, Enhanced energy release from homogeneous carbon nanotube-energetic material composites, *Sci. Adv. Mater.* **2016**, *8*, 164–170.

[7] B. Jin, R. F. Peng, S. J. Chu, Y. M. Huang, R. Wang. Study of the desensitizing effect of different [60] fullerene crystals on cyclotetramethylenetetranitramine (HMX), *Propellants Explos. Pyrotech.* **2010**, *33*, 454–458.

[8] J. L. Sabourin, D. M. Dabbs, R. A. Yetter, F. L. Dryer, I. A. Aksay, Functionalized graphene sheet colloids for enhanced fuel/propellant combustion, *ACS Nano.* **2009**, *3*, 3945–54.

[9] R. Li, J. Wang, J. P. Shen, C. Hua, G. C. Yang, Preparation and characterization of insensitive HMX/graphene oxide composites, *Propellants Explos. Pyrotech.* **2013**, *38*, 798–804.

[10] L. T. Le, M. H. Ervin, H. W. Qiu, B. E. Fuchs, W. Y. Lee, Graphene supercapacitor electrodes fabricated by inkjet printing and thermal reduction of graphene oxide, *Electrochem. Commun.* **2011**, *13*, 355–358.

[11] D. Khatayevich, T. Page, C. Gresswell, Y. Hayamizu, W. Grady, M. Sarikaya, Selective detection of target proteins by peptide-enabled graphene biosensor, *J. Small* **2014**, *10*, 1504–1504.

[12] V. Georgakilas, J. N. Tiwari, K. C. Kemp, J. A. Perman, A. B. Bourlinos, K. S. Kim, R. Zboril, Noncovalent functionalization of graphene and graphene oxide for energy materials, biosensing, catalytic, and biomedical applications, *Chem. Rev.* **2016**, *116*, 5464–5519.

[13] Z. Li, Y. Wang, Y. Zhang, L. Liu, S. J. Zhang, CL-20 hosted in graphene foam as a high-energy material with low sensitivity, *RSC Adv.* **2015**, *5*, 98925–98928.

[14] W. Zhang, Q. Luo, X. Duan, Y. Zhou, C. H. Pei, Nitrated graphene oxide and its catalytic activity in thermal decomposition of ammonium perchlorate, *J. Mater, Res. Bulletin.* **2014**, *50*, 73–78.

[15] L. Yu, H. Ren, X. Y. Guo, X. B. Jiang, Q. J. Jiao, A novel ε-HNIW-based insensitive high explosive incorporated with reduced graphene oxide, *J. Therm. Anal. Calorim.* **2014**, *117*, 1187–1199.

  

[16] X. Duan, S. ndrawirawan, H. Sun, S. Wang, Effects of nitrogen-, boron-, and phosphorus doping or co-doping on metal-free graphene catalysis, *J. Catal. Today.* **2015**, *249*, 184–191.
[17] H. B. Wang, T. Maiyalagan, X. Wang, Review on recent progress in nitrogen-doped graphene: synthesis, characterization, and its potential applications. *ACS Catal.* **2012**, *2*, 781–794.
[18] H. M. Jeong, J. W. Lee, W. H. Shin, Y. J. Choi, H. J. Shin, J. K. Kang, J. W. Choi, Nitrogen-doped graphene for high-performance ultracapacitors and the importance of nitrogen-doped sites at basal planes, *Nano Lett.* **2011**, *11*, 2472–2477.
[19] P. Chen, T. Y. Xiao, H. H. Li, J. J. Yang, Z. Wang, H. B. Yao, S. H. Yu, Nitrogen-doped graphene/ZnSe nanocomposites: hydrothermal synthesis and their enhanced electrochemical and photocatalytic activities, *ACS Nano.* **2012**, *6*, 712–719.
[20] Q. L. Yan, F. Q. Zhao, K. K. Kuo, X. H. Zhang, S. Zeman, L. T. DeLuca, Catalytic effects of nano additives on decomposition and combustion of RDX-, HMX-, and AP-based energetic compositions, *Prog. Energ. Combust.* **2016**, *57*, 75–136.
[21] D. Li, F. Q. Zhao, Q. Pan, H. X. Xu, Research on the thermal decomposition behavior of NEPE propellant containing CL-20, *J. Anal. Appl. Pyrolysis* **2016**, *121*, 121–127.
[22] R. Turcotte, M. Vachon, Q. S. M. Kwok, R. P. Wang, D. E. G. Jones, Thermal study of HNIW (CL-20), *Thermochim. Acta.* **2005**, *433*, 105–115.
[23] F. Q. Zhao, Combustion catalysts for solid propellant, National Defense Industry Press, **2016**, pp. 7–8.
[24] D. C. Marcano, D. V. Kosynkin, J. M. Berlin, A. Sinitskii, Z. Z. Sun, A. Slesarev, L. B. Alemany, W. Lu, J. M. Tour, Improved synthesis of graphene oxide, *ACS Nano.* **2010**, *4*, 4806–4814.
[25] L. Sun, L. Wang, C. G. Tian, T. X. Tan, Y. Xie, K. Y. Shi, M. T. Li, H. G. Fu, Nitrogen-doped graphene with high nitrogen level via a one-step hydrothermal reaction of graphene oxide with urea for superior capacitive energy storage, *RSC Adv.* **2012**, *2*, 4498–4506.
[26] Y. Wang, Y. Shao, D. W. Matson, J. Li, Y. Lin, Nitrogen-doped graphene and its application in electrochemical biosensing, *ACS Nano.* **2010**, *4*, 1790–1798.
[27] L. Liu, J. Lang, P. Zhang, B. Hu, X. B. Yan, Facile synthesis of $Fe_2O_3$ nano-dots@nitrogen-doped graphene for supercapacitor electrode with ultralong cycle life in KOH electrolyte, *ACS Appl.Mater.Inter.* **2016**, *8*, 9335 − 9344.
[28] B. J. Jiang, C. G. Tian, L. Wang, L. Sun, C. Chen, X. Z. Nong, Y. J. Qiao, H. G. Fu, Highly concentrated, stable nitrogen-doped graphene for supercapacitors: Simultaneous doping and reduction, *Appl. Surf. Sci.* **2012**, *258*, 3438–3443.
[29] H. X. Ma, J. R. Song, F. Q. Zhao, R. Z. Hu, H. M. Xiao, Non-isothermal reaction kinetics and computational studies on the properties of 2,4,6,8-tetranitro-2,4,6,8-tetraazabicyclo [3,3,1] onan-3,7-dione (TNPDU), *J. Phys. Chem. A.* **2007**, *111*, 8642–8649.
[30] T. Zhang, N. Zhao, J. C. Li, H. J. G, T. An, F. Q. Zhao, H. X. Ma, Thermal behavior of nitrocellulose-based superthermites: effects of nano-$Fe_2O_3$ with three morphologies, *RSC Adv.* **2017**, *7*, 23583–23590.
[31] J. H. Yi, F. Q. Zhao, B. Z. Wang, Q. Liu, C. Zhou, R. Z. Hu, Y. H. Ren, S. Y. Xu, K. Z. Xu, X. N. Ren, Thermal behaviors, non-isothermal decomposition reaction kinetics, thermal safety and burning rates of BTATz-CMDB propellant, *J. Hazard. Mater.* **2010**, *181*, 432–439.
[32] Y. Wang, Y. S. Shen, S. M. Zhu. N-doped graphene as a potential catalyst for the direct catalytic decomposition of NO, *Catal. Commun.* **2017**, *94*, 29–32.
[33] Y. F. Lan, X. Y. Li, Y. J. Luo, Research progress on application of graphene in energetic materials, *Chin. J. Explos. Propellants* **2015**, *38*, 1–7.
[34] T. L. Zhang, R. Z. Hu, Y. Xie, F. P. Li, The estimation of critical temperatures of thermal explosion for energetic materials using non-isothermal DSC, *Thermochim. Acta.* **1994**, *244*, 171–176.
[35] X. F. Yu. The effect of carbon nanotubes on the thermal decomposition of CL-20, *Chin. J. Explos. Propellants* **2004**, *27*, 78–80.
[36] UN. Recommendations on the Transport of Dangerous Goods. Manual of Tests and Criteria, UN-TDG, United Nations, New York and Geneva, **2009**.
[37] N. V. Muravyeva, V. G. Kiseleva, Cheaper, Faster, or Better: Are simple estimations of safety parameters of hazardous materials reliable? Comments on "Thermal behaviors, non-isothermal decomposition reaction kinetics, thermal safety and burning rates of BTATz-CMDB propellant by Zhao et al. (2010), *J. Hazard. Mater.* **2017**, *334*, 267–270.

Manuscript received: January 14, 2018
Accepted: July 1, 2018
Version of record online: November 28, 2018

  